International Journal of Hydrogen Energy 71 (2024) 1363–1372

Contents lists available at ScienceDirect

International Journal of Hydrogen Energy

journal homepage: www.elsevier.com/locate/he

Grand canonical Monte Carlo simulations of the hydrogen storage capacities of zeolite-templated carbon schwarzites at room temperature

M. López [a], M.B. Torres [b], I. Cabria [a,*]

[a] Departamento de Física Teórica, Atómica y Óptica, Universidad de Valladolid, ES-47011, Valladolid, Spain
[b] Departamento de Matemáticas y Computación, Universidad de Burgos, Burgos, Spain

ARTICLE INFO

Keywords:
Hydrogen storage
Methane storage
Carbon porous materials
Grand canonical Monte Carlo simulations

ABSTRACT

Fuel cell electric vehicles powered by hydrogen are zero-emissions vehicles. The on-board hydrogen storage is one of the main problems of these vehicles. Storage on solid porous materials is a promising method and a very active field of research. Nanoporous carbons are one of the main groups of solid porous materials. Schwarzites are a type of nanoporous carbons with a very complex porous structure. Grand Canonical Monte Carlo simulations of the hydrogen storage capacities of Zeolite-templated Carbon (ZTC) schwarzites and carbon-based slit-shaped pores at 298.15 K and in the pressure interval of 0.5-25 MPa have been carried out, analyzed and compared. Relationships between the structural parameters (density, porosity and pore size) and the storage capacities of ZTC schwarzites at room temperature and 25 MPa have been found and analyzed. The storage capacities of ZTC schwarzites are similar to the experimental and theoretical capacities of carbon-based materials.

1. Introduction

The climate change is mainly due to the emission of greenhouse gases. Most of the CO_2 emissions and pollution are caused by fossil fuel based road transport. The European Union aims to achieve a 60% reduction in transportation-related pollution by the year 2050, compared to the levels recorded in 1990 [1]. Hydrogen is an environmental-friendly alternative to fossil fuels. A transport based on the fuel cell electric vehicle powered by hydrogen would reduce the fossil fuel dependence, the emissions of greenhouse gases and the pollution. Hydrogen possesses a remarkably high specific energy. However, under standard conditions, it exhibits a low energy density. This poses a challenge for on-board storage of hydrogen in vehicles. Therefore, it is imperative to explore and develop methodologies that enable the storage of sufficient amounts of hydrogen. The technological objective is to create hydrogen-powered vehicles with a range autonomy comparable to fossil fuel-based vehicles, approximately 600 km.

The Department of Energy, DOE, has set on-board volumetric and gravimetric hydrogen storage targets for 2025 at 0.040 kg/L and 5.5 wt%, respectively [2]. The ultimate storage goals are even higher, aiming for 0.050 kg H_2/L and 6.5 wt.%. Another benchmark for storage capacities is provided by the 2018 Toyota Mirai, a commercial vehicle with tanks storing compressed hydrogen at 70 MPa within a total volume of 122.4 L. The Mirai boasts a gravimetric capacity of 5.7 wt%, a volumetric capacity of 0.040 kg/L, and a range autonomy of 312 miles (502 km) [3]. It is important to note that both the DOE and Toyota Mirai 2018 capacities represent deliverable or usable storage capacities.

Utilizing solid porous materials for hydrogen storage represents a promising avenue to achieve the aforementioned targets. This method involves the storage of hydrogen gas through physisorption on the surfaces of the pores within these materials. Ongoing research in the field focuses on identifying materials suitable for room temperature use that can store sufficient hydrogen for practical applications in hydrogen vehicle depots [4]. Compared to compression storage at similar pressures, the storage on solid porous materials demonstrates higher densities at low and moderate pressures. The notable high porosity of these materials positions them as promising candidates for on-board hydrogen storage.

Carbon-based nanostructured materials are a group of solid porous materials that have been widely studied in experiments and theoretical studies [5–12]. The exploration of various carbon nanostructures has yielded over 500 3d-periodic hypothetical carbon configurations, cataloged within the Samara Carbon Allotrope Database [13]. Most of these structures have been proposed in the last decade. Schwarzites are among those hypothetical carbon allotropes. They are carbon 3d periodic structures that reproduce a triple periodic surface minimum [14]. They are composed by sp^2-hybridized carbon atoms that form hexa-, hepta-, and octagons with a negative Gaussian curvature that corresponds to the minimal Schwarz surface [15,16]. Fullerenes have a

* Corresponding author.
E-mail address: ivan.cabria@uva.es (I. Cabria).

https://doi.org/10.1016/j.ijhydene.2024.05.256
Received 1 March 2024; Received in revised form 9 May 2024; Accepted 16 May 2024
Available online 26 May 2024

positive curvature and graphene, nanotubes and nanocones have zero curvature. There are schwarzites with P (primitive), D (diamond-like) and G (gyroid) surfaces [16–18].

The structure and electronic properties of some schwarzites (fcc-C36-2, fcc-C40-2 and fcc-C82-2) was investigated by Benedek et al. [19]. They concluded that these schwarzites have an stability similar to that of the C_60 molecule, and show insulating or metallic behavior, depending on their geometry. A molecular dynamics study of schwarzites was performed by Woellner et al. [20]. They compared the compressibility of four schwarzites (P688, P8bal, G688, G8bal). According to their results, it is possible to compress the schwarzites to half their size before they collapse. The interest to create these novel materials is driven by the predictions about their properties and possible technological applications such as battery electrodes, superconductors, catalysis, gas separation and gas storage [21].

Schwarzites have not yet been synthesized, although altered materials with local schwarzite-like properties have been isolated [22,23]. A possible synthesis method could consist on coating the inner surfaces of zeolites with sp^2 carbon. Zeolite-templated Carbon (ZTC) structures with crystalline forms of silicon dioxide could be used as a template for synthesizing schwarzites [24]. The process would consist on injecting a vapor of carbon-containing molecules. Carbon atoms would distribute on the surface of the zeolite pores, forming ZTCs. The resulting carbon surface has a negative curvature. A Monte Carlo theoretical method that mimics the mentioned synthesis method was developed by Braun et al. [24]. The comparison with ZTCs that had been previously studied using X-ray diffraction by Kim et al. [25] and Parmentier et al. [26], as the ZTC-FAU, justified this method. The method proposed by Braun et al. [24] predicted successfully the known ZTCs. The results of their research showed the relationship between ZTCs and schwarzites and proved that schwarzites are not purely hypothetical materials.

The porosity and density of many schwarzites suggest that these materials could store important amounts of hydrogen. Theoretical simulations of the storage capacities indicated that some schwarzites could have important gravimetric capacities at room temperature, 300 and 303 K, and moderate pressures, 5 and 10 MPa [15,27,28]. Hydrogen is storage by physisorption on the surfaces of the pores of schwarzites, as in other solid porous materials. This type of storage is reversible at room temperature.

This paper is devoted to ZTC schwarzites as geometric models of nanoporous carbons and as solid porous materials for hydrogen storage. Schwarzites are promising materials for hydrogen storage, due to their structural versatility and porosity. However, there are very few studies about their hydrogen storage capacities. Hence, the research of their storage capacities is innovative. Hydrogen storage capacities of ZTC schwarzites and slit-shaped pores have been investigated through Grand Canonical Monte Carlo (GCMC) simulations at room temperature. The structure of the paper is outlined as follows: Section 2 provides a detailed explanation of the GCMC simulations, while Section 3 presents and analyzes the results obtained from the simulations. Lastly, Section 4 is dedicated to drawing conclusions based on the findings.

2. Methodology and materials simulated

Grand Canonical Monte Carlo (GCMC) simulations were conducted to examine the adsorption of hydrogen molecules within schwarzites and carbon slit-shaped pores at 298.15 K and pressures between 0.5 and 25 MPa. Each GCMC simulation comprised one million iterations, with hydrogen storage capacities computed using the final 0.5 million iterations of each simulation. During each iteration, three potential trials were considered: moving, adding, or removing one molecule. Specifically, 40% of the trials involved the removal of one molecule, another 40% focused on the insertion of one molecule, and the remaining 20% pertained to the movement of one molecule. These trial percentages were determined through multiple test simulations.

The interactions between the hydrogen molecules have been calculated by means of the Lennard-Jones (LJ) interaction potential energy [29]. The interactions between the hydrogen molecules and the carbon atoms of the schwarzites have been also simulated with the LJ potential energy. The Steele potential energy [30] for graphene-H_2 has been utilized to calculate the interaction between the graphene layers of the slit-shaped pores and the H_2 molecules.

There are two interactions in the present GCMC simulations: carbon atom-H_2 or H_2–H_2. The LJ parameters ϵ and σ used in the simulations are those published by Rzepka et al. [31] The Steele potential energy of graphene–H_2 [30] also used the LJ parameters of the carbon atom-H_2 interaction. The Soave–Redlich–Kong, SRK, equation of state of hydrogen was used to calculate the chemical potential [32]. Two total hydrogen storage capacities, volumetric and gravimetric, are calculated in the GCMC simulations, according to the definitions previously published [33].

The designations, the coordinates of the atoms and the cell parameters and angles of the ZTC schwarzites were obtained from the data reported by Braun et al. [24]. The whole data set amounts to 66 schwarzites. The simulation cells of the schwarzites are non-orthorhombic. The simulation cells of the slit-shaped pores and schwarzites are large enough to contain between 100 and 600 molecules at moderate and high pressures, 5–25 MPa. The volume of the simulation cells of the schwarzites is about 100 000 Å^3. Their volume is, specifically, in the range 56 000–145 000 Å^3. The simulation cells of two of the schwarzites studied, RWY and AEI, are depicted in Fig. 1. The porosity of these two schwarzites can be noticed qualitatively in that Figure.

Fig. 2 is a depiction of the simulation cell of a slit-shaped pore used in the GCMC simulations. The pore is made of two flat and parallel graphene layers separated a distance called the pore width. The area of each graphene layer used in the simulations is 88.54 × 89.46 Å^2. The geometric or mathematical pore width of the simulated carbon slit-shaped pores varies between 5 and 22.5 Å and the volume of their simulation cells is in the range 47 500–199 000 Å^3, depending on the geometric pore width. The smallest distance between the center of a carbon atom of a graphene layer and the center of a carbon atom of the second layer is the geometric or mathematical width of a slit pore.

A comparison of the hydrogen storage capacities of a set of 14 schwarzites, obtained with 10^6 and 10^7 iterations can be found in Table 1. The hydrogen storage capacities of a simulation of 10 million iterations were computed using the last 5 million iterations. This comparison indicates that the difference between the capacities obtained in the simulations with one million iterations is very similar to those obtained using 10 million iterations. The simulations performed at one million iterations are about 10 times faster. Hence, the GCMC simulations of the present work were performed at one million iterations.

2.1. Calculation of the porosity and pore radius

The porosity and pore radius of the schwarzites have been calculated by means of the Zeo++ open software [35–41]. That software calculates the Voronoi network of a solid porous material using the Voronoi decomposition. The empty spaces within the structure of the material are represented by the calculated Voronoi network. The Zeo++ software reports two types of volume accessible to the gas molecules: The accessible volume, which is the volume of the solid porous material that the central point of a spherical probe can occupy, and the probe-occupiable volume, which is the volume of the solid porous material that can be occupied by the volume (by some points) of the spherical probe, not only by a single point [36]. There is a Figure in Ref. [36] that depicts these two types of volumes. The radius of the probe in the present calculations was 1.2 Å.

The porosity of a solid porous material is defined as the ratio between the volume accessible to the gas molecules and the simulation

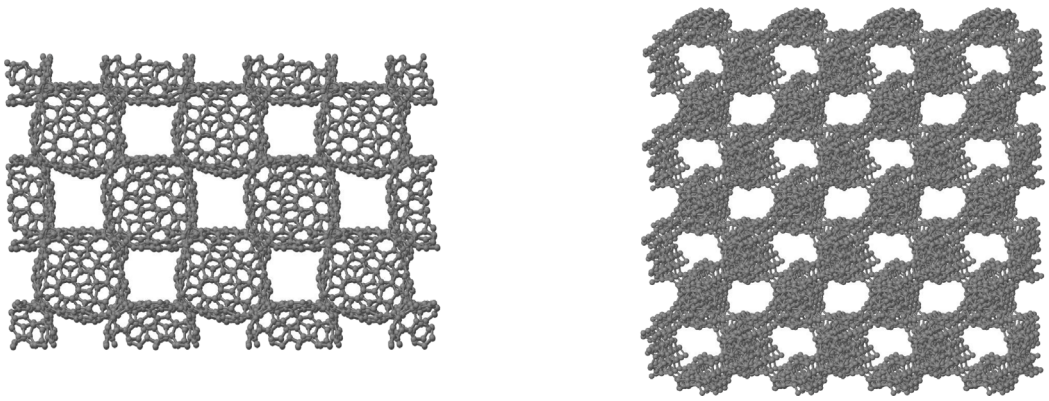

Fig. 1. (Color online) Simulation cell of the RWY (left panel) and AEI (right panel) schwarzites, plotted with the xmakemol software [34].

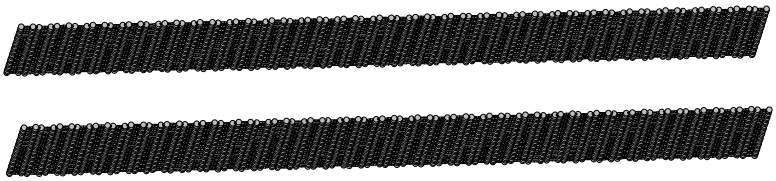

Fig. 2. (Color online) Simulation cell of a graphene slit-shaped pore, plotted with the xmakemol software [34].

Table 1
Comparison of the storage capacities of some schwarzites obtained with 10^6 and 10^7 iterations. Gravimetric capacities g_c are in wt. % units and volumetric capacities in kg H_2/L.

Schwarzite	$g_c 10^6$	$g_c 10^7$	$\lvert\Delta g_c\rvert$	$100\lvert\Delta g_c\rvert/g_c$	$v_c 10^6$	$v_c 10^7$	$\lvert\Delta v_c\rvert$	$100\lvert\Delta v_c\rvert/v_c$
AEI	1.062	1.060	0.002	0.19	0.012503	0.012485	0.000	0.14
AFY	0.847	0.848	0.001	0.12	0.012084	0.012091	0.000	0.06
EMT	1.855	1.859	0.004	0.22	0.016506	0.016500	0.000	0.04
ERI	1.149	1.161	0.012	1.03	0.012517	0.012644	0.000	1.00
FAU_1	1.776	1.771	0.005	0.28	0.016369	0.016325	0.000	0.27
GME	0.709	0.705	0.004	0.57	0.009039	0.008982	0.000	0.63
IRY	1.423	1.424	0.001	0.07	0.015844	0.015855	0.000	0.07
OSO	0.140	0.139	0.001	0.72	0.002439	0.002414	0.000	1.04
PUN	0.658	0.662	0.004	0.60	0.009373	0.009428	0.000	0.58
RWY	1.277	1.267	0.010	0.79	0.015784	0.015661	0.000	0.79
SAV	1.062	1.071	0.009	0.84	0.012498	0.012608	0.000	0.87
STW	1.078	1.082	0.004	0.37	0.013208	0.013257	0.000	0.37
SZR	0.208	0.208	0.000	0.00	0.003748	0.003753	0.000	0.13
UWY	1.701	1.711	0.010	0.58	0.015984	0.016082	0.000	0.61

cell volume. There are two types of porosities: the porosity from the accessible volume, P_{acc}, and the porosity from the probe-occupiable volume, P_{probe}. Ongari et al. [36] found that the probe-occupiable volume gave the closest results to the experimentally measured pore volumes for all the types of pores.

The pore radii have been calculated using the Zeo++ open software [35]. The software calculates the radius of the largest included sphere, R_i, the radius of the largest free sphere, R_f, and the radius of the largest included sphere along free sphere path, R_{if}. The largest included sphere is the largest sphere that fits into the largest pore of the porous material. The largest free sphere refers to the largest spherical probe capable of diffusing through the porous material. The largest included sphere along the free sphere path is the largest sphere that fits along the path where the largest free sphere was calculated. The definitions and pictures of these three radius can be found on different sources in the scientific literature [35–42]. Tables S1–S5 in the Supporting Information present the two types of porosities and the three types of pore radii of the schwarzites and slit-shaped pores, obtained using the Zeo++ software.

3. Results and discussion

3.1. GCMC hydrogen storage capacities of the schwarzites as a function of density

The storage capacities of solid porous materials depend on several magnitudes. One of those magnitudes is the density of the solid porous material. The densities of the schwarzites investigated in the present simulations are between 0.8 and 2.0 kg/L, while the densities of the slit-shaped pores are between 0.6 and 3.1 kg/L. The volumetric and gravimetric capacities at 298.15 K and 25 MPa of the schwarzites and slit-shaped pores have been gathered in Tables S1–S5 in the Supporting Information, together with their densities, and plotted in Fig. 3.

The results plotted in Fig. 3 show that the slit-shaped pores have larger volumetric and gravimetric capacities than the schwarzites with the same density. The volumetric capacities of the schwarzites are approximately constant below 1.0 kg/L and then they decrease, in general, as the density increases. The volumetric capacity of the slit-shaped pores is approximately constant for densities below 2.0 kg/L and then increases as the density increases, reaching a maximum,

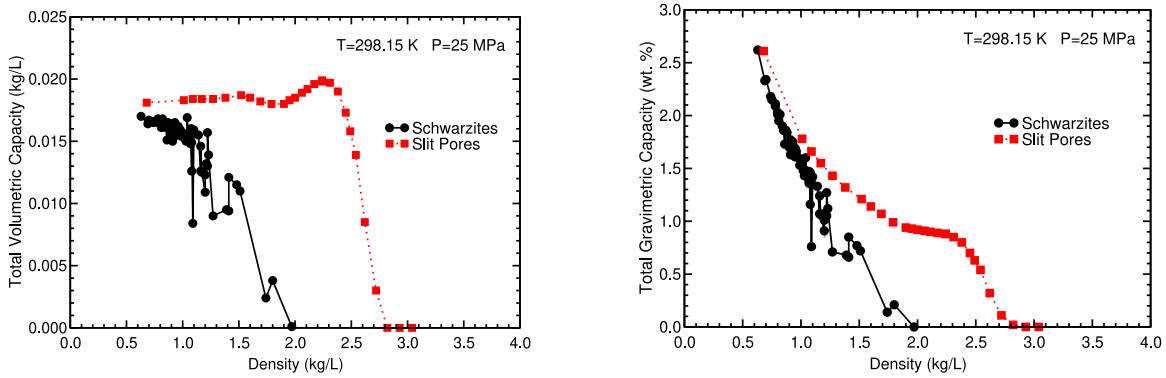

Fig. 3. (Color online) GCMC total volumetric and gravimetric capacities of the schwarzites (black solid symbols) and slit-shaped pores (red hollow symbols) at room temperature and 25 MPa as a function of the density.

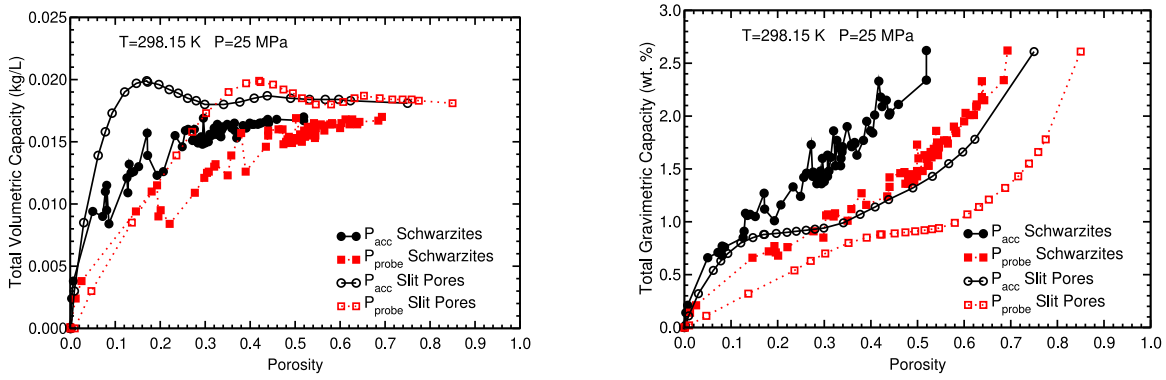

Fig. 4. (Color online) GCMC total volumetric and gravimetric capacities of the schwarzites (black solid symbols) and slit-shaped pores (red hollow symbols) at room temperature and 25 MPa as a function of the porosity.

and then decreases abruptly (See left panel of Fig. 3). The volumetric capacities of schwarzites and slit-shaped pores as a function of the density have in common that they are, approximately constant, at low densities. The gravimetric capacities of the schwarzites and slit-shaped pores decrease, in general, as the density increases.

These GCMC results suggest that a schwarzite with a low density, about 0.5 kg/L or less, might reach the DOE 2025 gravimetric target. However, at low densities, the volumetric capacities of schwarzites are approximately constant and about 0.016–0.017 kg H_2/L. Therefore, that hypothetical low density schwarzite would have a volumetric capacity of 0.016–0.017 kg H_2/L, far from the DOE 2025 volumetric target.

3.2. GCMC hydrogen storage capacities of the schwarzites as a function of porosity

The porosities of the schwarzites and slit-shaped pores have been calculated using the Zeo++ software [35]. Two types of porosities have been calculated and plotted in Fig. 4. The volumetric storage capacities of the schwarzites are, in general, smaller than those of the slit-shaped pores with the same porosity. In a few cases, with a low porosity, the volumetric capacities of the schwarzites are larger than those of the slit-shaped pores (See left panel of Fig. 4). The situation is the opposite in the case of the gravimetric capacities. The gravimetric storage capacities of the schwarzites are larger, even much larger, than the gravimetric capacities of the slit-shaped pores with the same porosity (See right panel of Fig. 4).

The volumetric capacities of the schwarzites and slit-shaped pores have in common that they increase as the porosity increases and reach, approximately, a constant value. The gravimetric capacities of the schwarzites and slit-shaped pores have in common that they, in general, increase monotonously as the porosity increases.

The dependence on the porosity obtained in these GCMC simulations suggest that a schwarzite with a high porosity, about 0.8 or more, might reach the DOE 2025 gravimetric target. That hypothetical high porosity schwarzite would have a volumetric capacity of about 0.016–0.017 kg H_2/L, far from the DOE 2025 volumetric target.

3.3. GCMC hydrogen storage capacities of the schwarzites as a function of pore size

The Zeo++ software [35] has been used in the present research to calculate the pore radii of the schwarzites and slit-shaped pores. Three types of pore radii have been calculated: The largest included sphere radius, the largest free sphere radius and the largest included sphere along free sphere path radius. The GCMC storage capacities of the schwarzites and slit-shaped pores at 298.15 K and 25 MPa have been compared with their three types of pore radius, obtained with the Zeo++ software, in Tables S1–S5 and Figs. 5 and 7.

It can be noticed in the upper and right panel of Fig. 5 that the GCMC total volumetric capacity of the schwarzites increases, in general, as the pore radius increases (any of the three types of pore radius) and then, it tends towards a constant value. As regards the GCMC total gravimetric capacity, it can be also noticed in the upper and left panel of Fig. 5 that this capacity increases, in general, as the three types of pore radius increases, not reaching a constant value. The dependence of the total gravimetric capacity on the pore radius is approximately linear. It is also important to appreciate in the upper panels of Fig. 5 that most of the radii R_i and R_{if} of the schwarzites coincide and that, in general, the radius R_f is smaller than the other two radii of the schwarzites.

The volumetric capacity of the slit pores experiences a rapid increase as the radius expands, reaching a peak before gradually converging towards a constant value (See the right and lower panel of Fig. 5).

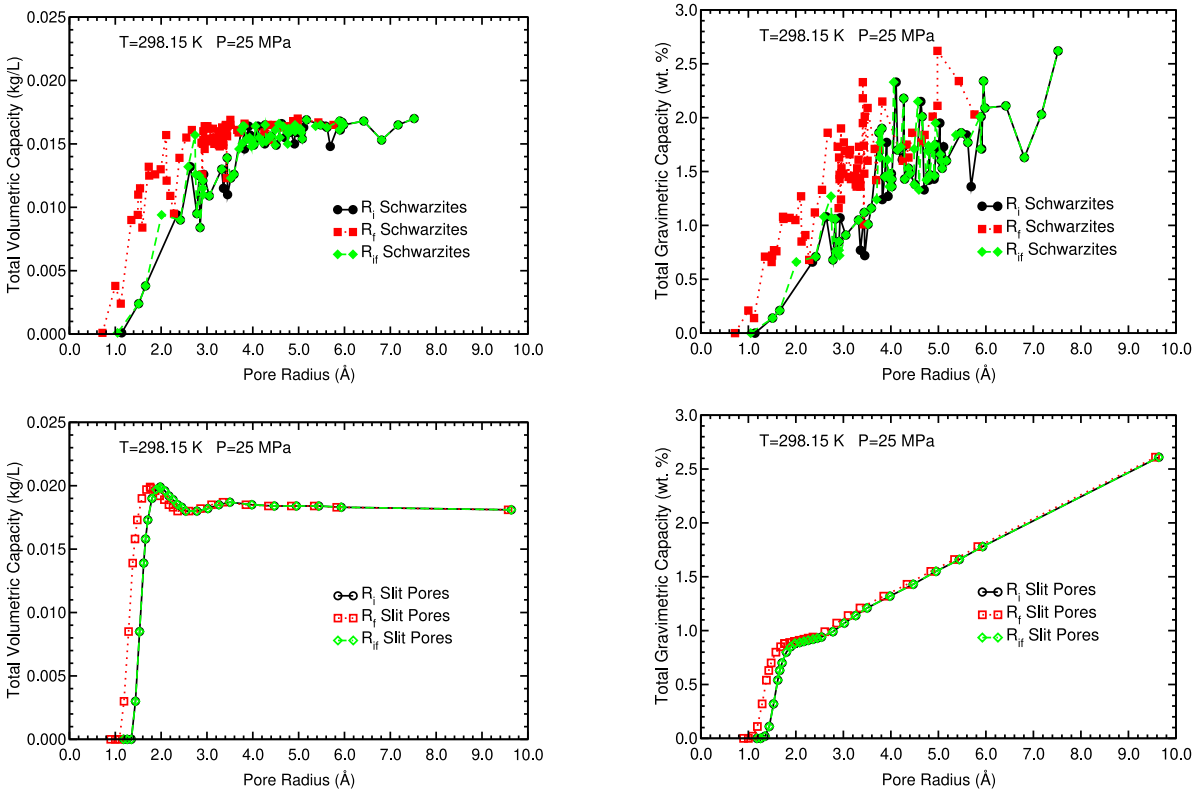

Fig. 5. (Color online) GCMC total volumetric and gravimetric capacities of the schwarzites (upper panels) and slit-shaped pores (lower panels) at room temperature and 25 MPa as a function of the three types of pore radius obtained with the Zeo++ software.

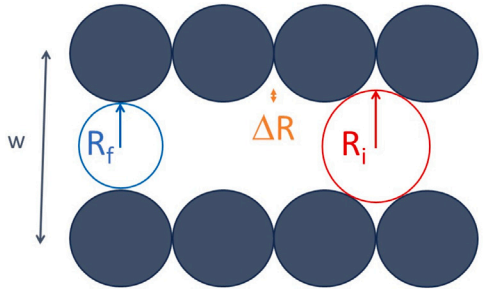

Fig. 6. (Color online) Depiction of the radii R_i and R_f and its difference ΔR of a slit-shaped pore whose geometric pore width is w. The gray solid circles represent the carbon atoms of the two layers of the slit-shaped pore.

The gravimetric capacity increases very fast as the radius increases and then it increases linearly (See the left and lower panel of Fig. 5). The radii R_i and R_{if} of the slit-shaped pores are identical, the radius R_f is smaller than the other two radii, as in the case of the schwarzites, and the difference between the radii R_i and R_f decreases as the geometric pore width w increases (See Tables S4 and S5). The radii R_i and R_f of an slit-shaped pore and its difference ΔR are depicted in Fig. 6.

In Fig. 7 a comparison of the storage capacities of the schwarzites and slit pores as a function of the same type of pore radius is shown. The volumetric capacity of a schwarzite is smaller than the volumetric capacity of a slit-shaped pore with the same radius (any of the three types of radius). Only in the short interval of the smallest radii, below 1.4 Å, the volumetric capacity of a schwarzites is larger. In that interval of the smallest radii, the capacities are very small or almost null.

As regards the gravimetric capacity, for radius R_i or R_{if} below 3.5 Å, the gravimetric capacity of a schwarzite is, in general, smaller than the gravimetric capacity of a slit pore with the same R_i or R_{if} pore radius (See Fig. 7). For radius R_i or R_{if} above 3.5 Å, the gravimetric capacity of a schwarzite is, in general, larger than the gravimetric capacity of a slit pore with the same pore radius. The dependence of the gravimetric capacity of schwarzites and slit pores on the pore radius R_f shows that the gravimetric capacity of a schwarzite is, in general, larger than the gravimetric capacity of a slit pore with the same R_f pore radius, in the whole range of values of R_f studied.

The comparison of the storage capacities of schwarzites as a function of their diameters D_x and $w_x = D_x + 2\, r_{vdW}$, with x = i, f or if, and the storage capacities of the slit pores as a function of their geometric pore width w is plotted in Fig. 8. r_{vdW} is the van der Waals radius of a carbon atom, which is about 1.7 Å. The diameter w_x is an approximated mathematical or geometric pore diameter: The distance between the centers of two opposing carbon atoms on the surface of the pore. It can be noticed in Tables S4 and S5 that the geometric pore width w of a slit pore is approximately equal to w_f.

It can be noticed in Fig. 8 that very few schwarzites and slit pores with the same diameter D_x (x = i, f or if) and geometric pore width w, have the same volumetric or gravimetric capacity. A second comparison is between the schwarzite capacities vs. w_x and the slit-shaped pore capacities vs. w. This second comparison also reveals that very few schwarzites with the same diameter w_x and slit pores with the same geometric pore width w, have the same volumetric capacity. As regards the gravimetric capacity, some slit-shaped pores and schwarzites with the same w and w_x, have the same gravimetric capacity.

The comparison of the schwarzite capacities vs. R_x with the slit pore capacities vs. R_x (x = i, f or if) (See Fig. 7), the schwarzites capacities vs. D_x with the slit pore capacities vs. D_x and the schwarzites capacities vs. w_x with the slit pore capacities vs. w (See Fig. 8), shows that schwarzites and slit pores with the same pore size (R_x, D_x, w_x or w) do not have, in general, the same storage capacities, according to the present simulations. To conclude that schwarzites and slit pores with the same pore size have the same storage capacities, the schwarzite and slit pore curves in Fig. 7 or Fig. 8 should overlap in all the range

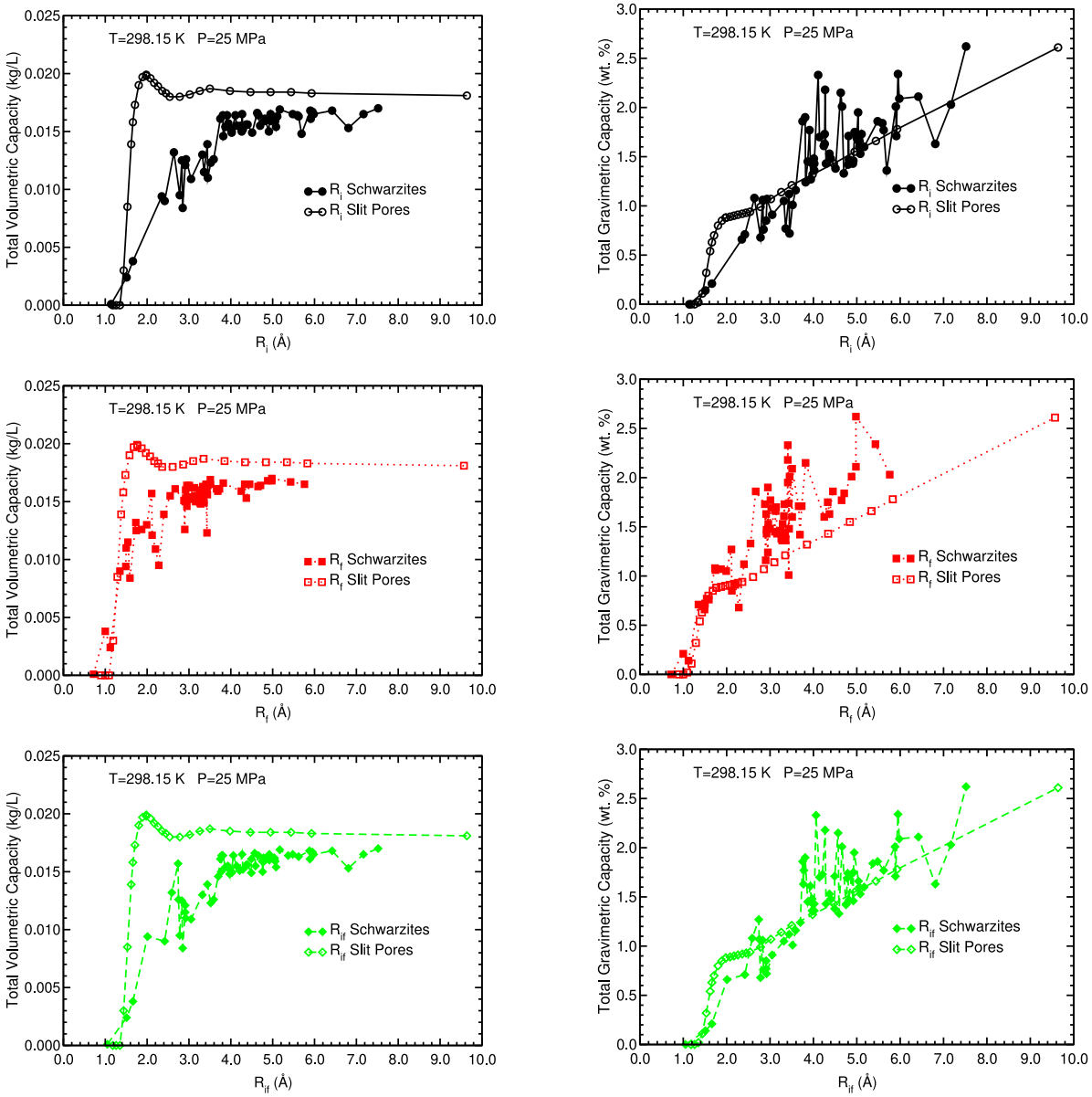

Fig. 7. (Color online) GCMC total volumetric and gravimetric capacities of the schwarzites (black solid symbols) and slit-shaped pores (red hollow symbols) at room temperature and 25 MPa as a function of the three types of radius.

of pore size studied. They do not overlap: A few schwarzites have the same volumetric capacity that slit pores with the same pore size and some schwarzites have the same gravimetric capacity that slit pores with the same pore size.

The volumetric capacities of the slit pores vs. pore size (R_x, D_x, w_x or w) have a maximum, while the volumetric capacities of the schwarzites vs. pore size do not have a maximum, as can be noticed in Figs. 7 and 8. The maximum volumetric capacity corresponds to a slit pore with a geometric pore width of 6.78 Å. The volumetric capacities of schwarzites and slit pores vs. pore size have in common that they increase fast and then they tend towards a constant value, as the pore size increases. The gravimetric capacities of slit pores increase fast and then increase linearly as the pore size increases. The gravimetric capacities of the schwarzites also increase linearly with the pore size, but with many oscillations around an average straight line.

Table 2 is a summary of the storage capacities and structural parameters of the studied ZTC schwarzites plotted in Figs. 3–5, 7 and 8.

3.4. A simple relationship between the gravimetric capacity and the volumetric capacity and the density of the schwarzites

It can be shown that the gravimetric capacity is a simple and approximate function of the volumetric capacity and the density of the adsorbent material, in this case, the density of the schwarzite. The mass of stored hydrogen in the simulation cell is equal to $M_H = v_c V$, where V is the volume of the simulation cell. The mass of the adsorbent material is $M_{ads} = \rho V$, where ρ is the volumetric mass density of the adsorbent material. In the present case, ρ is the density of the schwarzite. Inserting these two equations into the definition of the gravimetric capacity, $100 M_H/(M_H + M_{ads})$ (See Ref. [33]), leads to the following equation:

$$g_c = \frac{100 v_c}{v_c + \rho}. \quad (1)$$

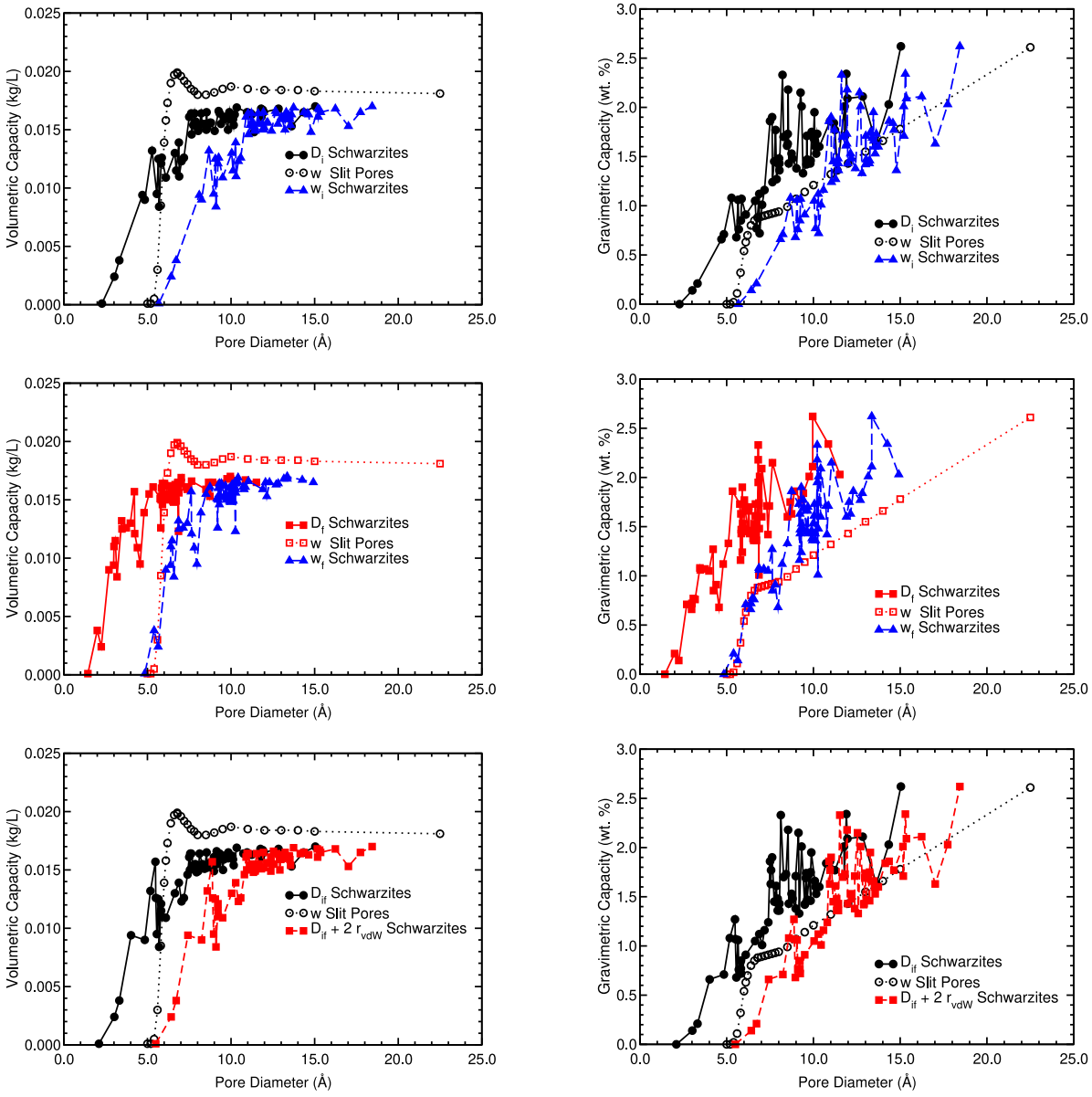

Fig. 8. (Color online) GCMC total volumetric and gravimetric capacities of the schwarzites (solid symbols) as a function of the pore diameters D_x and w_x (x = i, f or if), and of slit-shaped pores (hollow symbols) as a function of the geometric pore width, w, at room temperature and 25 MPa.

Table 2
Summary of the gravimetric (in wt.%) and volumetric (in kg/L) storage capacities, densities (in kg/L), porosities (dimensionless) and pore radii (in Å) of the ZTC schwarzites.

g_c	v_c	Density	P_{acc}	P_{probe}	R_i	R_f	R_{if}
0.0–2.6	0.0–0.017	0.5–2.0	0.0–0.52	0.0–0.69	1.1–7.3	0.85–6.0	1.1–7.3

The volumetric capacities v_c at 25 MPa and the densities of the schwarzites are below 0.02 kg H_2/L and 2.0 kg/L, respectively. Hence, it is a valid approach to consider that $v_c + \rho \approx \rho$ and Eq. (1) turns into

$$g_c \approx \frac{100 v_c}{\rho} \,. \tag{2}$$

The total gravimetric capacities obtained in the simulations have been compared with the approximate gravimetric capacities obtained using Eq. (2). The results have been plotted in Fig. 9. This figure proves that the mathematical approach or relationship between g_c, v_c and ρ, Eq. (2), is a reasonable assumption.

In a previous publication [6], an equation similar to Eq. (2) was derived for slit pores, nanotubes and torusenes:

$$g_c \approx \frac{100 f v_c}{\sigma_{\text{adsorbent}}} \,, \tag{3}$$

where $f = V/S$ is the volume/surface ratio and $\sigma_{\text{adsorbent}}$ is the surface mass density of the adsorbent material. The slit pores, nanotubes and torusenes have very well defined surfaces, while the schwarzites have

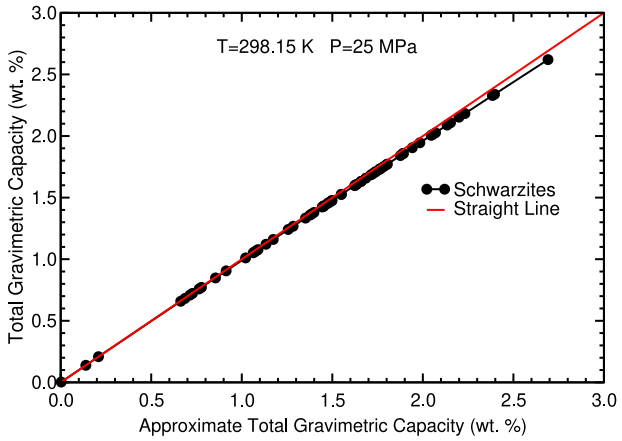

Fig. 9. (Color online) GCMC total gravimetric capacity vs. approximated total gravimetric capacity of the schwarzites at room temperature and 25 MPa.

not well defined surfaces and hence, the volumetric mass density of the adsorbent material, ρ, must be used in Eq. (2) instead of $\sigma_{\text{adsorbent}}/f$. It was shown in Ref. [6] that Eq. (3) was a valid approach for slit pores, nanotubes and torusenes. In the present publication it has been shown that an equivalent equation, Eq. (2), is also a sound approach.

3.5. GCMC hydrogen storage capacities of schwarzites as a function of the pressure

GCMC simulations of the volumetric and gravimetric hydrogen storage capacities of the ZTC schwarzites were performed at pressures ranging from 0.5 to 25 MPa and at a temperature of 298.15 K. The GCMC schwarzites capacities are also compared with the GCMC storage capacities of several carbon slit-shaped with geometric pore widths between 5 and 22.5 Å. Some of the GCMC slit-shaped capacities used in the comparison were previously published [6].

The results of the simulations are shown in Fig. 10. The panels of that figure show the total volumetric and gravimetric hydrogen storage capacities at room temperature, 298.15 K, vs. the pressure, the so-called isotherms, of four ZTC schwarzites (black solid symbols) and four slit-shaped pores (red hollow symbols). The four schwarzites are RHO, ERI, BSV and OSO. RHO and OSO have the highest and lowest storage capacities among the ZTC schwarzites studied, respectively. The capacities of ERI and BSV are intermediate between those of RHO and OSO. The storage capacities of CHA are almost null (See Table S1).

The volumetric isotherms of the schwarzites are between those of the slit-shaped pores with a geometric pore width w between 5.6 and 6.15 Å. The volumetric isotherms of OSO (lowest isotherm) and RHO schwarzite (highest isotherm) coincide approximately with those of the slit pores of geometric width 5.6 and 6.15 Å, respectively. The gravimetric isotherms of the schwarzites are between those of the slit-shaped pores with a geometric width between 5.6 and 22.5 Å. The gravimetric isotherms of OSO schwarzite (lowest isotherm) and RHO (highest isotherm) coincide approximately with those of the slit pores of geometric width 5.6 and 22.5 Å, respectively.

3.6. Comparison with experiments on carbon-based materials and with simulations of other schwarzites

The GCMC storage capacities of the schwarzites are compared with the experimental storage capacities of some carbon nanostructures and activated carbons at different pressures and at room temperature or close to room temperature in Table 3. Kunowsky et al. [43] measured the hydrogen storage capacities of a wide range of KOH-activated carbon fibers (ACFs). Their findings revealed that, at 298 K and 20 MPa, the maximum total volumetric capacity of the ACFs was 0.0171 kg/L. In a separate study, Xu et al. [44] measured the gravimetric capacities of diverse carbon-based porous materials, including activated carbons, graphitic carbon nanofibers, single-walled carbon nanotubes and single-walled carbon nanohorns. They observed that, at 303 K and 10 MPa, the gravimetric capacity of these materials was below 0.7 wt.%. Ströbel et al. [45] conducted hydrogen storage experiments on various carbon nanostructures, reporting gravimetric capacities ranging from 0.1 to 1.6 wt. % at 296.15 K and 10 MPa. Jordá-Beneyto et al. [46] measured the volumetric isotherm of KUA5, a well-known activated carbon, at 298 K, obtaining volumetric capacities of 0.0100 and 0.0167 kg/L at 10 and 20 MPa, respectively.

The highest volumetric capacities of the schwarzites at 10 and 20 MPa and room temperature, which correspond to the RHO schwarzite, are about 15%–20% smaller than the experimental volumetric capacities of KUA5 at the same conditions, as can be noticed in Table 3. The gravimetric capacities of the schwarzites at 10 and 20 MPa are within the range of the experimental gravimetric capacities of carbon-based porous materials (See Table 3).

The GCMC storage capacities of the ZTC schwarzites is also compared with the theoretical capacities of other schwarzites in Table 3. Krasnov et al. carried out theoretical simulations of the hydrogen storage capacities of four D-schwarzites, a type of schwarzite [15], and of the P216-schwarzite [27]. They obtained that the gravimetric storage capacities at 300 K and 10 MPa of the D168, D224, D360, D480 and P216 schwarzites are 3.0, 3.34, 6.4, 7.65 and 4.6 wt.%, respectively. Borges and Galvao [28] did GCMC simulations of the storage capacities of H_2 on some schwarzites. They found that the P688 schwarzite has a gravimetric storage capacity of 0.34 wt.% at 303 K and 5 MPa.

The range of the gravimetric capacities of the ZTC schwarzites studied at 5 MPa is 0.03–0.74 wt.% and this range is in agreement with the P688 gravimetric capacity theoretical result of 0.34 wt.% (See Table 3). The gravimetric storage capacity of ERI is the closest one to the gravimetric capacity of P688. However, the gravimetric storage capacities of the ZTC schwarzites at 10 MPa are much smaller than the theoretical capacities of D-schwarzites and the P-216 schwarzite.

The experimental porosities of activated carbons range, according to experiments [47], between 0.03 and 0.96. These values can be compared with the porosities of the ZTC schwarzites in Tables S1–S5, which range from 0.0 to 0.52 for P_{acc} and from 0.0 to 0.69 for P_{probe}.

4. Conclusions

GCMC simulations of the hydrogen storage capacities at room temperature and pressures between 0.5 and 25 MPa of ZTC schwarzites and carbon-based slit-shaped pores have been carried out and analyzed. The provided GCMC results are predictions of the storage capacities of ZTC schwarzites at room temperature. The volumetric capacities of ZTC schwarzites are comparable to those of narrow slit-shaped pores (width in the interval 5.6–6.15 Å), while the gravimetric capacities are comparable to the capacities of narrow and wide slit-shaped pores (width in the interval 5.6–22.5 Å).

The dependence of the GCMC storage capacities at 298.15 K and 25 MPa of the ZTC schwarzites and carbon-based slit-shaped pores with the density, porosity and pore size has been analyzed. The gravimetric capacities of both types of materials increase as the inverse of the density, the porosity or the pore size increases. The volumetric capacities of both types of materials tend towards a constant value as the inverse of the density, the porosity or the pore size increases. This means that there are general trends of the storage capacities of carbon based pores that do not depend on the shape of the pore.

According to the present GCMC simulations, a ZTC schwarzite designed with a density of 0.4–0.5 kg/L or a porosity of 0.9 or with pores with radii of 20 Å could reach the DOE gravimetric target [2], 5.5 wt.%, at room temperature and 25 MPa or higher pressures. However, the DOE volumetric target, 0.040 kg H_2/L, could not be reached, because

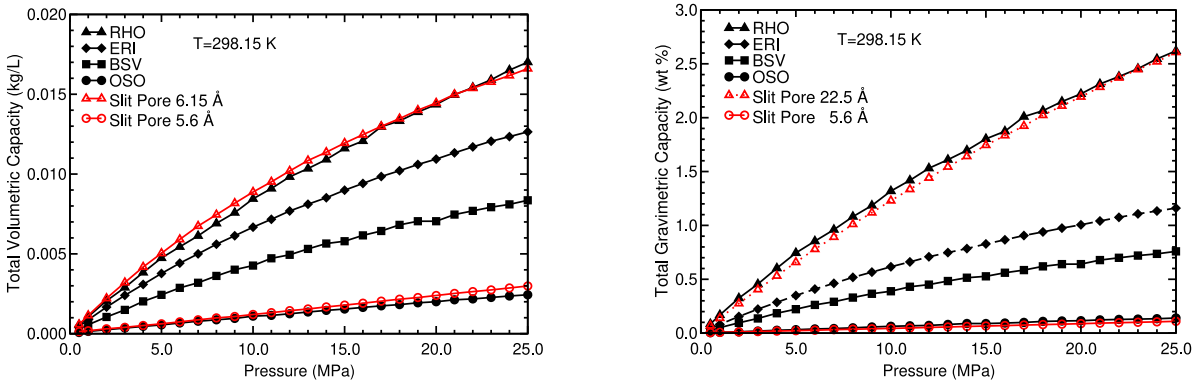

Fig. 10. (Color online) GCMC total volumetric and gravimetric capacities of the schwarzites (black solid symbols) and slit-shaped pores (red hollow symbols) vs. pressure at room temperature.

Table 3
Experimental and theoretical total hydrogen volumetric (in kg/L) and gravimetric (in wt.%) storage capacities of carbon-based porous materials. Temperature and pressure are in K and MPa, respectively. Ex. and Th. stand for experimental and theoretical results, respectively.

Material	v_c	g_c	T	P	Source
P688	–	0.34	303	5	Th. Borges and Galvao [28]
ERI	0.0038	0.35	298.15	5	Th. Present GCMC
ZTC Schwarzites	0.0006–0.0047	0.03–0.74	298.15	5	Th. Present GCMC
Carbon-based materials	–	<0.7	303	10	Ex. Xu et al. [44]
Carbon-based materials	–	0.1–1.6	296.15	10	Ex. Ströbel et al. [45]
AC KUA5	0.0100	–	298	10	Ex. Jordá-Beneyto et al. [46]
D-schwarzites	–	3.00–7.65	300	10	Th. Krasnov et al. [15]
P216	–	4.6	300	10	Th. Krasnov et al. [27]
ZTC Schwarzites	0.0011–0.0084	0.06–1.32	298.15	10	Th. Present GCMC
ACFs	0.0171	1.3	298	20	Ex. Kunowsky et al. [43]
AC KUA5	0.0167	–	298	20	Ex. Jordá-Beneyto et al. [46]
ZTC schwarzites	0.0020–0.0144	0.12–2.22	298.15	20	Th. Present GCMC

the volumetric storage capacity tends towards a constant value as the inverse of the density, the porosity or the pore size increases.

A ZTC schwarzite and a slit pore with the same pore size do not have, in general, the same storage capacities. The storage capacities of ZTC schwarzites are similar to those of carbon-based slit-shaped pores obtained in GCMC simulations and also to the experimental storage capacities of activated carbons and a variety of carbon-based porous materials. The ZTC schwarzites could be used as geometrical models of carbon-based materials with a complex porous structure, such as activated carbons.

CRediT authorship contribution statement

M. López: Conceptualization, Data curation, Formal analysis, Investigation, Methodology, Project administration, Resources, Software, Supervision, Validation, Visualization, Writing – original draft, Writing – review & editing. **M.B. Torres:** Conceptualization, Data curation, Formal analysis, Investigation, Methodology, Project administration, Resources, Software, Supervision, Validation, Visualization, Writing – original draft, Writing – review & editing. **I. Cabria:** Conceptualization, Data curation, Formal analysis, Investigation, Methodology, Project administration, Resources, Software, Supervision, Validation, Visualization, Writing – original draft, Writing – review & editing.

Declaration of competing interest

The authors declare that they have no known competing financial interests or personal relationships that could have appeared to influence the work reported in this paper.

Acknowledgments

This research has been financially supported by the MICINN research project from Spain (Grant PGC2018-093745-B-I00), the Junta de Castilla y León research project, Spain (Grant VA124G18), and the University of Valladolid, Spain. The authors would like to express their gratitude for the use of the computer facilities at the Centro de Procesado de Datos - Parque Científico of the University of Valladolid. The simulations cells and the graphs have been plotted with the xmakemol [34] and grace [48] software, respectively.

Appendix A. Supplementary data

Supplementary material related to this article can be found online at https://doi.org/10.1016/j.ijhydene.2024.05.256.

References

[1] Net Zero Emissions by 2050 scenario (NZE). 2022, https://www.iea.org/reports/global-energy-and-climate-model/net-zero-emissions-by-2050-scenario-nze, [Accessed 27 February 2024].

[2] Office of Energy Efficiency & Renewable Energy, Fuel Cell Technologies Office. DOE technical targets for onboard hydrogen storage for light-duty vehicles. 2018, https://www.energy.gov/eere/fuelcells/doe-technical-targets-onboard-hydrogen-storage-light-duty-vehicles, [Accessed 27 February 2024].

[3] Broom DP, Webb CJ, Fanourgakis GS, Froudakis GE, Trikalitis PN, Hirscher M. Concepts for improving hydrogen storage in nanoporous materials. Int J Hydrog Energy 2019;44(15):7768–79. http://dx.doi.org/10.1016/j.ijhydene.2019.01.224.

[4] Hynek S, Fuller W, Bentley J. Hydrogen storage by carbon sorption. Int J Hydrog Energy 1997;22:601–10.

[5] Macili A, Vlamidis Y, Pfusterschmied G, Leitgeb M, Schmid U, Heun S, Veronesi S. Study of hydrogen absorption in a novel three-dimensional graphene structure: Towards hydrogen storage applications. Appl Surf Sci 2023;615:156375. http://dx.doi.org/10.1016/j.apsusc.2023.156375.
[6] Caviedes D, Cabria I. Grand Canonical Monte Carlo simulations of the hydrogen storage capacities of slit-shaped pores, nanotubes and torusenes. Int J Hydrog Energy 2022;47:11916–28. http://dx.doi.org/10.1016/j.ijhydene.2022.01.229.
[7] Cabria I, Lebon A, Torres M, Gallego L, Vega A. Hydrogen storage capacity of Li-decorated borophene and pristine graphene slit pores: a combined ab-initio and quantum-thermodynamic study. Appl Surf Sci 2021;562:150019. http://dx.doi.org/10.1016/j.apsusc.2021.150019.
[8] Zhang Y, Zhang L, Pan H, Wang H, Li Q. Li-decorated porous hydrogen substituted graphyne: A new member of promising hydrogen storage medium. Appl Surf Sci 2021;535:147683. http://dx.doi.org/10.1016/j.apsusc.2020.147683.
[9] Karki S, Chakraborty SN. A Monte Carlo simulation study of hydrogen adsorption in slit-shaped pores. Microporous Mesoporous Mater 2021;317:110970. http://dx.doi.org/10.1016/j.micromeso.2021.110970.
[10] Wang Y, Xu G, Deng S, Wu Q, Meng Z, Huang X, Bi L, Yang Z, Lu R. Lithium and sodium decorated graphdiyne as a candidate for hydrogen storage: First-principles and grand canonical Monte Carlo study. Appl Surf Sci 2020;509:144855. http://dx.doi.org/10.1016/j.apsusc.2019.144855.
[11] Wang Y, Wu Q, Deng S, Ma R, Huang X, Bi L, Yang Z. Hydrogen storage in Na-decorated H_4,4,4-graphyne: A density functional theory and Monte Carlo study. Appl Surf Sci 2019;495:143621. http://dx.doi.org/10.1016/j.apsusc.2019.143621.
[12] Cheng Y-H, Zhang C-Y, Ren J, Tong K-Y. Hydrogen storage in Li-doped fullerene-intercalated hexagonal boron nitrogen layers. Front Phys 2016;11(5):113101. http://dx.doi.org/10.1007/s11467-016-0559-4.
[13] Hoffmann R, Kabanov AA, Golov AA, Proserpio DM. Homo citans and carbon allotropes: For an ethics of citation. Angew Chem Int Edn 2016;55:10962–76.
[14] Phillips R, Drabold DA, Lenosky T, Adams GB, Sankey OF. Electronic structure of schwarzite. Phys Rev B 1992;46:1941–3.
[15] Krasnov PO, Shkaberina GS, Kuzubov AA, Kovaleva EA. Molecular hydrogen sorption capacity of D-schwarzites. Appl Surf Sci 2017;416:766–71. http://dx.doi.org/10.1016/j.apsusc.2017.04.161.
[16] Huang MZ, Ching WY, Lenosky T. Electronic properties of negative-curvature periodic carbon surface. Phys Rev B 1993;47:1593–606.
[17] Vanderbilt D, Tersoff J. Negative-curvature fullerene analog of C60. Phys Rev Lett 1992;68:511–3.
[18] Townsend SJ, Lenosky TJ, Muller DA, Nichols CS, Elser V. Negatively curved graphical sheet model of amorphous carbon. Phys Rev Lett 1992;69:921–4.
[19] Benedek G, Bernasconi M, Cinquanta E, D'Alessio L, de Corato M. The topological background of Schwarzite physics. In: Cataldo F, Graovac A, Ori O, editors. The mathematics and topology of fullerenes. carbon materials: chemistry and physics. Dordrecht: Springer; 2011, p. 217–47. http://dx.doi.org/10.1007/978-94-007-0221-9_12, Ch. 12.
[20] Woellner CF, Botari T, Peri E, Galvão DS. Mechanical properties of Schwarzites - a fully atomistic reactive molecular dynamics investigation. MRS Adv 2018;3:451–6. http://dx.doi.org/10.1557/adv.2018.124.
[21] Terrones H, Terasaki M. Curved nanostructured materials. New J Phys 2003;5:126.
[22] Bourgeois LN, Bursill LA. High-resolution transmission electron microscopic study of nanoporous carbon consisting of curved single graphitic sheets. Phil Mag A 1997;76:753–68.
[23] Barborini E, Piseri P, Milani P. Negatively curved spongy carbon. Appl Phys Lett 2002;81:3359–61. http://dx.doi.org/10.1063/1.1516635.
[24] Braun E, Lee Y, Moosavi SM, Barthel S, Mercado R, Baburin IA, Smit B. Generating carbon schwarzites via zeolite-templating. Proc Natl Acad Sci USA 2018;115:E8116–24.
[25] Kim K, Lee T, Kwon Y, Seo Y, Song J, Park JK, Lee H, Park JY, Ihee H, Cho SJ, Ryoo R. Lanthanum-catalysed synthesis of microporous 3D graphene-like carbons in a zeolite template. Nature 2016;535:131–5. http://dx.doi.org/10.1038/nature18284.
[26] Parmentier J, Gaslain FOM, Ersem O, Centeno TA, Solovyov LA. Structure and sorption properties of a zeolite-templated carbon with the EMT structure type. Langmuir 2014;30:297–307.
[27] Krasnov PO, Shkaberina GS, Polyutov SP. Molecular hydrogen sorption capacity of P216-schwarzite: PM6-D3, MP2 and QTAIM approaches. Comput Mater Sci 2022;209:111410. http://dx.doi.org/10.1016/j.commatsci.2022.111410.
[28] Borges DD, Galvao DS. Schwarzites for natural gas storage: A grand-canonical Monte Carlo study. MRS Adv 2018;3:115–20. http://dx.doi.org/10.1557/adv.2018.190.
[29] Lennard-Jones JE. On the determination of molecular fields. Proc R Soc (Lond) A 1924;106:463–77. http://dx.doi.org/10.1098/rspa.1924.0082.
[30] Steele WA. The physical interaction of gases with crystalline solids: I. Gas-solid energies and properties of isolated adsorbed atoms. Surf Sci 1973;36:317–52.
[31] Rzepka M, Lamp P, de la Casa-Lillo MA. Physisorption of hydrogen on microporous carbon nanotubes. J Phys Chem B 1998;102:10894–8. http://dx.doi.org/10.1021/jp9829602.
[32] Soave G. Equilibrium constants from a modified Redlich-Kwong equation of state. Chem Eng Sci 1972;27:1197–203.
[33] Cabria I. Grand canonical Monte Carlo simulations of the hydrogen and methane storage capacities of novel but MOFs at room temperature. Int J Hydrog Energy 2024;50:160–77. http://dx.doi.org/10.1016/j.ijhydene.2023.06.298.
[34] Hodges MP. XMakemol: a program for visualizing atomic and molecular systems. 2007, https://www.nongnu.org/xmakemol, [Accessed 27 February 2024]. (Last version: 5.16).
[35] Haranczyk M. Zeo++: an open source software for performing high-throughput geometry-based analysis of porous materials and their voids. 2017, http://www.zeoplusplus.org, [Accessed 27 February 2024]. (Last version: 0.3).
[36] Ongari D, Boyd PG, Barthel S, Witman M, Haranczyk M, Smit B. Accurate characterization of the pore volume in microporous crystalline materials. Langmuir 2017;33(51):14529–38. http://dx.doi.org/10.1021/acs.langmuir.7b01682.
[37] Martin RL, Haranczyk M. Structure models of crystalline porous polymers: Construction, characterization and design. Cryst Growth Des 2014;14:2431–40. http://dx.doi.org/10.1021/cg500158c.
[38] Pinheiro M, Martin RL, Rycroft CH, Jones A, Iglesia E, Haranczyk M. Characterization and comparison of pore landscapes in crystalline porous materials. J Mol Graph Model 2013;44:208–19. http://dx.doi.org/10.1016/j.jmgm.2013.05.007.
[39] Pinheiro M, Martin RL, Rycroft CH, Haranczyk M. High accuracy geometric analysis of crystalline porous materials. CrystEngComm 2013;15:7531–8. http://dx.doi.org/10.1039/C3CE41057A.
[40] Martin RL, Smit B, Haranczyk M. Addressing challenges of identifying geometrically diverse sets of crystalline porous materials. J Chem Inf Model 2012;52:308–18. http://dx.doi.org/10.1021/ci200386x.
[41] Willems TF, Rycroft CH, Kazi M, Meza JC, Haranczyk M. Algorithms and tools for high-throughput geometry-based analysis of crystalline porous materials. Microporous Mesoporous Mater 2012;149(1):134–41. http://dx.doi.org/10.1016/j.micromeso.2011.08.020.
[42] Foster MD, Rivin I, Treacy MMJ, Delgado Friedrichs O. A geometric solution to the largest-free-sphere problem in zeolite frameworks. Microporous Mesoporous Mater 2006;90:32–8. http://dx.doi.org/10.1016/j.micromeso.2005.08.025.
[43] Kunowsky M, Marco-Lozar JP, Cazorla-Amorós D, Linares-Solano A. Scale-up activation of carbon fibres for hydrogen storage. Int J Hydrog Energy 2010;35:2393–402. http://dx.doi.org/10.1016/j.ijhydene.2009.12.151.
[44] Xu W-C, Takahashi K, Matsuo Y, Hattori Y, Kumagai M, Ishiyama S, Kaneko K, Iijima S. Investigation of hydrogen storage capacity of various carbon materials. Int J Hydrog Energy 2007;32:2504–12.
[45] Ströbel R, Jorissen L, Schliermann T, Trapp V, Schutz W, Bohmhammel K, Wolf G, Garche J. Hydrogen adsorption on carbon materials. J Power Sources 1999;84:221. http://dx.doi.org/10.1016/S0378-7753(99)00320-1.
[46] Jordá-Beneyto M, Suárez-García F, Lozano-Castelló D, Cazorla-Amorós D, Linares-Solano A. Hydrogen storage on chemically activated carbons and carbon nanomaterials at high pressures. Carbon 2007;45:293–303.
[47] Blankenship LS, Mokaya R. Modulating the porosity of carbons for improved adsorption of hydrogen, carbon dioxide, and methane: a review. Mater Adv 2022;3:1905–30. http://dx.doi.org/10.1039/d1ma00911g.
[48] Turner PJ, Grace Development Team. Grace: a WYSIWYG 2D plotting tool. 2015, http://plasma-gate.weizmann.ac.il/Grace. [Accessed 27 February 2024]. (Last version: 5.1.25).